Scattering on triply periodic minimal surfaces—the effect of the topology, Debye–Waller, and molecular form factors

Piotr Garstecki and Robert Hoyst

Citation: The Journal of Chemical Physics **113**, 3772 (2000); doi: 10.1063/1.1287426
View online: http://dx.doi.org/10.1063/1.1287426
View Table of Contents: http://scitation.aip.org/content/aip/journal/jcp/113/9?ver=pdfcov
Published by the AIP Publishing

Scattering on triply periodic minimal surfaces—the effect of the topology, Debye–Waller, and molecular form factors

Piotr Garstecki[a] and Robert Hołyst
Institute of Physical Chemistry PAS and College of Science, Dept. III, Kasprzaka 44/52, 01-224 Warsaw, Poland

(Received 6 January 2000; accepted 1 June 2000)

We compute scattering patterns for four triply periodic surfaces (TPS). Three minimal—Schwarz P ($Im\bar{3}m$), Schwarz D—diamond ($Pn\bar{3}m$), Schoen G—gyroid ($Ia\bar{3}d$), and one nodal S1 ($Ia\bar{3}d$). Simple approximations are adopted to examine the influence of the molecular form factor, and the Debye–Waller factor on the scattering pattern. We find that the Debye–Waller factor has a much smaller influence on the scattering intensities of TPS than on the intensities of the lamellar structure consisting of parallel surfaces. This is caused by an almost spherelike distribution of normal vectors for TPS. We give a simple formula that allows a comparison of the experimental scattering data with the data for the P, D, G mathematical surfaces. Finally, the spectra of the two surfaces G and S1 of the same space group symmetry and different topologies are compared. It is found that in the case of the more complex S1 structure the intensities of the first two peaks are very small. © *2000 American Institute of Physics.* [S0021-9606(00)50633-3]

I. INTRODUCTION

The small-angle x-ray and neutron scattering experiments are widely used to determine the symmetry and structure of self-assembling systems. Still, in the case of the structures formed by a surfactant surface in binary (with water) and ternary (with oil and water) mixtures, it is often hard to exactly determine the type of topological phase in the system. The pioneering work in this field was done by Luzzati *et al.*[1,2] They showed that the mesoscopic structure of surfactant aggregates could be more complex than spheres (micelles in microemulsion), cylinders (hexagonal phases), or planes (lamellar phases). Scriven[3] was the first one to propose triply periodic minimal surfaces as a possible realization of the bicontinous structures in ternary mixtures. Since then the scattering techniques were often used to monitor the structural phase transitions; see, for example, Refs. 4–8. All these works indicate that the SAXS and SANS are powerful tools that provide information on the symmetry of the structures present in the system. Yet, the x-ray diffraction data are not always conclusive: due to the generally small number of reflections, an accurate reconstruction of an electronic map of the cubic cell is often impossible. Even once the space group is rigorously established, there is still the question as to the identity of the minimal surface and thus the topology of the structure. For example, the first report on the observation of a periodic surface in block copolymers was done in 1986 by Thomas *et al.*[9] They identified the surface dividing A monomer rich and B monomer rich domains as the Schwartz minimal surface D. It took nine years until Hajduk *et al.*[10] in 1995 gave the correct identification of this structure as the G gyroid minimal surface (both surfaces are shown in Fig. 1). It proves that even for structures of different space symmetry groups, the exact determination of them may be very difficult and thus a theoretical analysis of the scattering spectra is still needed.

The first example of a triply periodic minimal surface (TPMS) free of self-intersections was introduced by Schwarz in 1865.[11] It is now known as the Schwarz diamond D surface. Since then strong theoretical arguments of symmetry such as the minimization of the bending energy of the symmetric bilayer supported the picture of such surfaces as the model of the surfactant bilayers. These theoretical procedures lead to the discovery of many new TPMS.[12] Theoretically the world of self-assembly is very rich in many simple and complex periodic structures of cubic symmetry. Many of them have the same space group symmetry, even though their topologies are drastically different. It would thus be interesting to be able to determine from SANS or SAXS both the symmetry and topology of the structure in surfactant solutions.

Mackay[13] and Anderson[14] have computed the scattering amplitudes for few mathematical surfaces. Still the results had no practical impact since the computation method did not take into account the bilayer thickness and fluctuations. In the case of the G structure, both the molecular form and Debye–Waller factors have been included in the calculation conducted by Clerc and Dubois-Violette,[15] which provided very good fits with experimental data. Still, as the authors concluded in their work,[15] the calculations were made for a surfactant bilayer with a constant density independent of the local curvature, and the Debye–Waller factor characterized only isotropic displacement of the film while real surfactant bilayers fluctuate only in the direction normal to the surface.[16] In the two other directions the membrane has a liquid structure.

It was our original motivation to adopt a simple model of the density of the scatterers in the surfactant layer and its

[a]Electronic mail: garst@saka.ichf.edu.pl

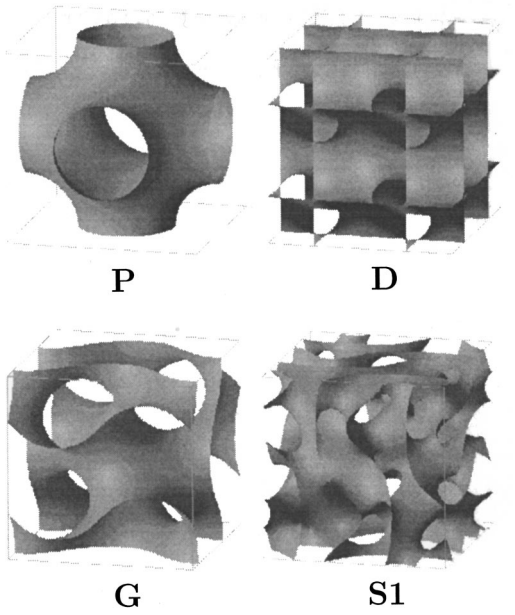

FIG. 1. The zero width—mathematical surfaces in the unit cells of the P (top left), D (top right), G (bottom left), and S1 (bottom right) structures.

dynamics to present a method of obtaining scattering intensities for various structures that can be compared with the experimental results and thus help in determining the structure type.

Figure 1 shows the zero width-mathematical surfaces of the P, D, G, and S1 structures. To compute the scattering intensities for these TPS, we adopt a simple numerical procedure. The surfaces are determined by the condition $f(\mathbf{r})=0$, where $f(\mathbf{r})$ is a scalar field, in three cases (P, D, G) taken from a minimization procedure conducted by Góźdź and Holyst[12] and in one case (S1) from the nodal approximation.[17] Then the surfaces are triangulated. Each triangle becomes a point scatterer. Then at each point we introduce a surfactant molecule. For simplicity, the calculations are shown for a very simple nucleus density distributed uniformly along the molecule. Then each scatterer is allowed to fluctuate independently. We find that fluctuations do reduce the intensity of the scattering, yet this effect is surprisingly small and much less important than in the case of smectic liquid crystals.[18] Finally, we have made an attempt to compare two structures (G and S1) of the same space symmetry group $Ia\bar{3}d$. G is the structure with a simple topology (Euler characteristic per unit cell $\chi=-8$), while S1[17] is a much more complex one ($\chi=-48$). The S1 structure is also more complex than the S surface[19] for which $\chi=-40$. The scattering intensities including the molecular form factor and the Debye–Waller factor indicate, that in the case of complex structures, the short wave vector peaks are rather small, while higher-order peaks become dominant. Thus, the shift of the intensities toward longer wave vectors may indicate a higher complexity of the system.

The paper is organized as follows. Section II is devoted to the presentation of the model of the density of the scatters and numerical methods used in the computation of the scattering intensities. In the third section the results for the mathematical surfaces, finite width surfaces and fluctuating surfaces are shown and discussed. The fourth section contains the summary of our results and discussion.

II. MODEL

The triply periodic minimal and nodal surfaces divide the volume into two continuous and separate subvolumes. In binary mixtures two physical realizations of a minimal surface are possible. One is a direct phase in which a water film is centered on the surface and surfactant molecules are filling the two subspaces. The second case is an invert phase in which the surface is decorated by a bilayer of surfactant and the two subspaces are filled with water. In our work we focus on the invert phase.

The binary mixture can be modeled by a concentration field function $f(\mathbf{r})$ taking positive values in one subvolume and negative in the other. Still, the fact that the field function takes opposite signs in the two subspaces has no experimental significance but is only related to the mathematical procedure. The condition $f(\mathbf{r})=0$ determines the mathematical surface decorated by the surfactant molecules. In the case of the minimal surfaces P, D, G we have the concentration field from the minimization procedure.[12] It is given on a cubic lattice inside a unit cell. Typically the lattice spacing is of the order of 1/50 of the linear size of a cell d.

Once we determine values of the field $f(\mathbf{r})$ on the lattice inside the unit cell, we triangulate the surface on which $f(\mathbf{r})=0$. In this way we obtain a set of, typically 50 000, triangles covering the whole surface in a unit cell. In real mixtures the surfactant molecule head covers the area of the order of 50 Å^2. The linear size of a unit cell is of the order of $d\sim 200$ Å or bigger. In simple structures the surface area per unit cell is of the order of $5d^2$. In more complex ones it is bigger than $10d^2$.[12] This gives aproximately about 10 000 or more of the surfactant molecules per unit cell, which shows, that triangles covering the surfaces are small enough to obtain reliable spectra. The scatterers used in computing the scattering intensities are positioned in the middle of each triangle and given the weight equal to the surface area of the triangle. Also, each scatterer is associated with a unit vector normal to the surface, which allows us to take into account the effects of the local curvature.

Our interest is focused on the surface contrast. To our knowledge it is best realized in neutron scattering experiments when the hydrophobic surfactant chains are deuterated. If we take $\hat{\rho}(\mathbf{r})$ as the density of the scatterers in the unit cell, the neutron diffraction intensity, $I(\mathbf{k})$ is the Fourier transform of the density–density correlation function,

$$I(\mathbf{k})=\langle A(\mathbf{k})A^*(\mathbf{k})\rangle = \int d\mathbf{r}\int d\mathbf{r}'\langle\hat{\rho}(\mathbf{r})\hat{\rho}(\mathbf{r}')\rangle\exp[i\mathbf{k}(\mathbf{r}-\mathbf{r}')]. \quad (1)$$

In a unit cell the density operator $\hat{\rho}$ can be written in the following form:

$$\hat{\rho}(\mathbf{r})=\int d\xi\,\delta\{f[\mathbf{r}-u(\mathbf{r})\mathbf{n}(\mathbf{r})-\xi\mathbf{n}(\mathbf{r})]\}\rho_M(\xi). \quad (2)$$

Here $\mathbf{n}(\mathbf{r})$ is a unit vector paralel to the gradient of the field $f(\mathbf{r})$, $u(\mathbf{r})$ is the fluctuation amplitude, and $\rho_M(\xi)$ is the molecular density operator equal to

$$\rho_M(\xi)=\theta\left(|\xi|-\frac{L}{2}\right), \tag{3}$$

where L is the width of the hydrocarbon part of the surfactant bilayer. We assume that the $f(\mathbf{r})=0$ surface is located in the middle of the surfactant bilayer. As we see from Eq. (2) the surfaces fluctuate along their normals.[16] The average in Eq. (1) is over the distribution of the fluctuation amplitudes $u(\mathbf{r})$.

We assume that the multiple scattering of the incident beam in the sample can be neglected. In general, the x-ray multiple scattering can be neglected because the Thompson cross section for electron–photon scattering is very small. In the case of neutron scattering the same assumption is fully justified.

The scattering amplitude,

$$A(\mathbf{k})=\int d\mathbf{r}\exp[i\mathbf{kr}]\hat{\rho}(\mathbf{r}), \tag{4}$$

can be represented by the sum over the points on the surface and the integral along the vectors normal to the surface $\Sigma_{j=1}^{N}s_j\int d\xi$:

$$A(\mathbf{k})=\sum_{j=1}^{N}s_j\int d\xi'\exp[i\mathbf{k}(\mathbf{r}_j+\xi'\mathbf{n}_j)]\times\int d\xi\,\delta[f(\mathbf{r}_j+\xi'\mathbf{n}_j-u_j\mathbf{n}_j-\xi\mathbf{n}_j)]\rho_M(\xi), \tag{5}$$

where s_j is the surface area of the jth triangle, and $\mathbf{n}_j$ is a unit vector normal to the surface at the jth point. Please note that the summation over j in Eq. (5) is over the surface given by $f(\mathbf{r})=0$. This point is justified because the total number of scatterers on the surface $f(\mathbf{r})=0$ is the same as on any surface $f(\mathbf{r}-\xi\mathbf{n})=0$ for $|\xi|<L/2$. On a flat surface the surface area $s_j(\xi)$ per one scattering rode is constant and equal to s_j. When the surface bends the $s_j(\xi)$ is given by the formula $s_j(\xi)=s_j[1+2H\xi+K\xi^2]$,[20] where ξ is negative if the displacement is toward the closest center of curvature, positive otherwise, H is the mean curvature, and K is the Gaussian curvature for $\xi=0$ at the jth point. In this way the surface density of scatterers increases towards the center of curvature and decreases otherwise, but the total number of scatterers remains constant.

Now the amplitude can be rewritten in the following form:

$$A(\mathbf{k})=\sum_{j=1}^{N}s_j\exp[i\mathbf{kr}_j]\exp[i\mathbf{kn}_ju_j]\frac{\sin\left(\mathbf{kn}_j\frac{L}{2}\right)}{\mathbf{kn}_j\frac{L}{2}}. \tag{6}$$

Assuming no correlations between fluctuation amplitudes, we obtain the scattering intensity $I(\mathbf{k})$:

$$I(\mathbf{k})=\left[\sum_{j=1}^{N}s_j\cos(\mathbf{kr}_j)\exp\left(-\frac{1}{2}(\mathbf{kn}_j)\langle u^2\rangle\right)\frac{\sin\left(\mathbf{kn}_j\frac{L}{2}\right)}{\mathbf{kn}_j\frac{L}{2}}\right]^2+\left[\sum_{j=1}^{N}s_j\sin(\mathbf{kr}_j)\exp\left(-\frac{1}{2}(\mathbf{kn}_j)\langle u^2\rangle\right)\frac{\sin\left(\mathbf{kn}_j\frac{L}{2}\right)}{\mathbf{kn}_j\frac{L}{2}}\right]^2, \tag{7}$$

where $\langle u^2\rangle$ can be calculated from the theory of elasticity for membranes. The equation for $\langle u^2\rangle$ is given in the work of Bruinsma:[16]

$$\langle u^2\rangle\simeq\frac{k_BTd^3}{\sqrt{\kappa\bar{\bar{\kappa}}}}\left(\frac{\Gamma_1}{\sqrt{1+\Gamma_2d^2k_BT/\bar{\bar{\kappa}}}}+\frac{\Gamma_3}{\sqrt{1-\Gamma_4d^2k_BT/\bar{\bar{\kappa}}}}\right) \tag{8}$$

where κ is the Helfrich bending energy, $\bar{\bar{\kappa}}\sim\kappa L^2$ and $\Gamma_1-\Gamma_4$ are positive constants. Without the precise knowledge of these constants we are not able to compute the $\langle u^2\rangle$. Therefore we have calculated the scattering intensities for several fluctuation amplitudes $\sqrt{\langle u^2\rangle}$ from 5% to 25% of the bilayer width.

Since we do not compute the scattering patterns for any specific surfactant molecule, the width of the hydrocarbon part of the surfactant bilayer has been estimated upon geometrical considerations. We have varied the volume fraction of the surfactant bilayer in the unit cell from 40% to 60%.

III. RESULTS

First of all we have computed the scattering intensities in the case of $\langle u^2\rangle=0$ and $L=0$ from Eq. (7), performing the summation over the surface in the unit cell. The first columns of Tables I–III present the scattering intensity $J_0(\mathbf{k})$ peaks for the zero width ($L=0$), nonfluctuating ($\langle u^2\rangle=0$) mathematical surfaces of TPMS P, D, G. The signs given in parentheses are the signs of the amplitudes. To obtain the magnitude of an amplitude form these data, one has to take a square root of the intensity. The signs and magnitudes allow us to determine the electron density map, which, in general, can be compared with transmission electron microscopy data.

The results are in agreement with the space group symmetry of these surfaces. The peaks prohibited by the reflection conditions are smaller than 10^{-7}. The structure factor of these surfaces makes a few of the allowed peaks also very weak. In the tables only the values of the intensities of the allowed peaks are presented. They are in a very good agrement, both in the signs and magnitudes, with the amplitudes presented by Anderson[14] and Clerc and Dubois-Violette.[15] Most of them differ at most by 0.1% and only a few differ by up to 4%. Comparing the data for the D surface one has to be extremely careful. Anderson has computed the scattering amplitudes for the lattice fundamental region, which has the surface area equal to one-half the area of the surface in the unit cell. Thus, the amplitudes have to be multiplied by 2 and next squared to be compared with the scattering intensities presented in Tables I–III. Another thing that has to be re-

TABLE I. The scattering intensities for the P structure, including the influence of the molecular form factor. V_L is the volume occupied by the surfactant tails in the unit cell of linear size d. The signs in the parentheses correspond to the signs of the amplitudes. The first column contains the intensities for the mathematical surface.

Scattering intensities including molecular factor Schwarz P structure			
hkl	$V_L=0$	$V_L=0.4\cdot d^3$	$V_L=0.6\cdot d^3$
000	(+)5.502 263	(+)5.502 263	(+)5.502 263
110	(−)0.202 135	(−)0.164 180	(−)0.117 490
200	(−)0.296 284	(−)0.192 640	(−)0.088 380
211	(+)0.208 205	(+)0.107 770	(+)0.029 580
220	(−)0.001 792	(−)0.000 690	(−)0.000 030
222	(−)0.164 350	(−)0.039 200	(−)0.000 020
310	(+)0.009 716	(+)0.003 080	(+)0.000 160
321	(−)0.047 421	(−)0.008 480	(+)0.000 140
330	(+)0.046 434	(+)0.004 000	(−)0.001 860
332	(+)0.078 049	(+)0.003 040	(−)0.003 780
400	(+)0.060 235	(+)0.007 780	(−)0.000 780
411	(−)0.058 761	(−)0.005 260	(+)0.001 750
420	(+)0.024 880	(+)0.001 390	(−)0.001 430
422	(+)0.064 302	(+)0.001 450	(−)0.003 530
431	(−)0.000 543	(−)0.000 001	(+)0.000 110
433	(−)0.071 706	(+)0.000 060	(+)0.002 700
440	(−)0.025 412	(+)0.000 000	(+)0.001 160
442	(−)0.010 239	(+)0.000 020	(+)0.000 240
444	(+)0.067 399	(−)0.001 910	(−)0.000 090

membered, is that in order for the (hkl) indices to obey the reflection conditions of the space group $Pn\bar{3}m$, they have been divided by 2, which has not been done in the work of Anderson.

The same tables I–III contain scattering intensities for finite width surfaces. Out of several widths we have presented the ones that occupy 40% and 60% of the unit cell volume, since these values are comparable to the volume fraction of surfactants in real binary mixtures. The molecular form factor:

$$\mathcal{F}_M^j = \frac{\sin\left(\mathbf{kn}_j \frac{L}{2}\right)}{\mathbf{kn}_j \frac{L}{2}}, \tag{9}$$

at the jth point reduces the intensity of the Bragg peaks, as is evident from the table.

TABLE II. The scattering intensities for the D structure. The legend is the same as in Table I.

Scattering intensities including molecular factor Schwarz D—diamond structure			
hkl	$V_L=0$	$V_L=0.4\cdot d^3$	$V_L=0.6\cdot d^3$
000	(+)14.763 758	(+)14.763 758	(+)14.763 758
110	(+)0.917 469	(+)0.656 950	(+)0.387 790
111	(+)0.938 575	(+)0.562 200	(+)0.234 510
200	(−)0.275 791	(−)0.137 630	(−)0.038 020
211	(+)0.179 375	(+)0.060 200	(+)0.004 740
220	(+)0.267 707	(+)0.059 010	(+)0.000 080
221	(+)0.311 919	(+)0.053 800	(−)0.000 620
222	(+)0.334 889	(+)0.025 520	(−)0.008 490

TABLE III. The scattering intensities for the G structure. The legend is the same as in Table I.

Scattering intensities including molecular factor Gyroid structure			
hkl	$V_L=0$	$V_L=0.4\cdot d^3$	$V_L=0.6\cdot d^3$
000	(+)9.589 390	(+)9.589 390	(+)9.589 390
211	(+)0.428 246	(+)0.301 730	(+)0.159 600
220	(+)0.185 458	(+)0.116 270	(+)0.047 400
321	(−)0.009 438	(−)0.003 870	(−)0.000 400
332	(+)0.225 676	(+)0.052 090	(−)0.000 060
400	(−)0.113 892	(−)0.043 300	(−)0.004 440
420	(−)0.109 526	(−)0.030 250	(−)0.000 190
422	(+)0.076 736	(+)0.015 650	(−)0.000 090
431	(+)0.036 024	(+)0.006 500	(−)0.000 090
440	(−)0.009 829	(−)0.000 640	(+)0.000 970
442	(+)0.000 010	(+)0.000 001	(−)0.000 000
444	(+)0.169 050	(+)0.001 640	(−)0.008 840

A very simple analysis can explain the influence of the molecular form factor on the scattering intensity. It is based on the observation that the P, D, G surfaces have almost spherelike distribution of normal vectors.[21] We now consider a scattering intensity function for a simple cubic structure with a sphere inside a unit cell with a sphere radius equal to 1:

$$I_0(\mathbf{k}) = (2\pi)^2 \left(\int_0^\pi d\theta \sin\theta \exp[i|\mathbf{k}|\cos\theta] \right)^2. \tag{10}$$

It is important to remember that the ''sphere crystal'' is an abstract model. One should not look for any physical analogies of it. It only serves as a model giving correct predictions of the molecular form factor influence on the scattering pattern. We have found that the scattering intensity function for this structure, including the molecular factor divided by the function (10):

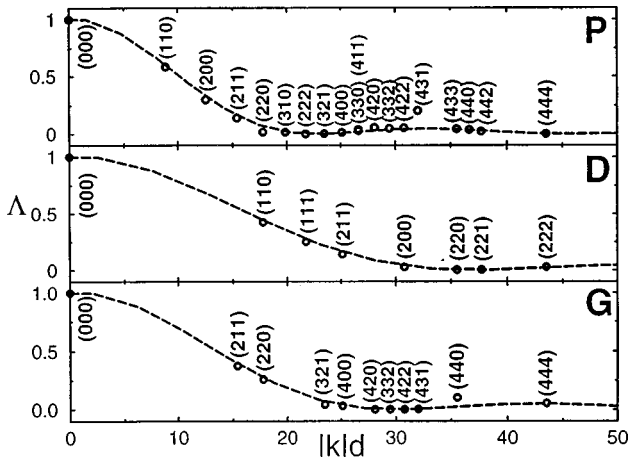

FIG. 2. The dashed lines show the functions $\Lambda_S(\mathbf{k})$ [Eq. (11)] computed in the maxima of $I_0(\mathbf{k})$ [Eq. (10)]. The ratios $\Lambda_{P,D,G}(\mathbf{k})$ [Eq. (12)] computed at the Bragg peak positions of the P, D, G structures are represented by empty circles.

TABLE IV. The scattering intensities for the P structure, including the influence of the Debye–Waller factor. $\sqrt{\langle u^2\rangle}$ is the fluctuation amplitude and L is the width of the hydrocarbon part of the surfactant bilayer. The signs in the parentheses correspond to the signs of the amplitudes. The first column contains the intensities for the mathematical surface.

Scattering intensities including Debye–Waller factor Schwarz P structure			
hkl	$\sqrt{\langle u^2\rangle}=0$	$\sqrt{\langle u^2\rangle}=0.05\cdot L$	$\sqrt{\langle u^2\rangle}=0.25\cdot L$
000	(+)5.502 263	(+)5.502 263	(+)5.502 263
110	(−)0.202 135	(−)0.199 122	(−)0.137 220
200	(−)0.296 284	(−)0.287 517	(−)0.131 687
211	(+)0.208 205	(+)0.199 030	(+)0.062 852
220	(−)0.001 792	(−)0.001 687	(−)0.000 247
222	(−)0.164 350	(−)0.150 182	(−)0.014 833
310	(+)0.009 716	(+)0.009 014	(+)0.001 458
321	(−)0.047 421	(−)0.042 689	(−)0.003 102
330	(+)0.046 434	(+)0.040 556	(+)0.001 041
332	(+)0.078 049	(+)0.066 159	(+)0.001 065
400	(+)0.060 235	(+)0.053 423	(+)0.002 933
411	(−)0.058 761	(−)0.051 334	(−)0.001 718
420	(+)0.024 880	(+)0.021 405	(+)0.000 348
422	(+)0.064 302	(+)0.053 702	(+)0.000 600
431	(−)0.000 543	(−)0.000 446	(−)0.000 001
433	(−)0.071 706	(−)0.055 546	(−)0.000 111
440	(−)0.025 412	(−)0.019 980	(−)0.000 052
442	(−)0.010 239	(−)0.007 821	(−)0.000 016
444	(+)0.067 399	(+)0.047 018	(+)0.000 011

$$\Lambda_S=\frac{I(\mathbf{k})}{I_0(\mathbf{k})}=\frac{\left(\int_0^{\pi} d\theta \sin\theta \exp[i|\mathbf{k}|\cos\theta]\dfrac{\sin\left(|\mathbf{k}|\dfrac{L}{2}\cos\theta\right)}{|\mathbf{k}|\dfrac{L}{2}\cos\theta}\right)^2}{\left(\int_0^{\pi} d\theta \sin\theta \exp[i|\mathbf{k}|\cos\theta]\right)^2}, \tag{11}$$

is comparable to the analogous function calculated for the periodic surfaces P, D, G:

TABLE V. The scattering intensities for the D structure. The legend is the same as in Table IV.

Scattering intensities including Debye–Waller factor Schwarz D—diamond structure			
hkl	$\sqrt{\langle u^2\rangle}=0$	$\sqrt{\langle u^2\rangle}=0.05\cdot L$	$\sqrt{\langle u^2\rangle}=0.25\cdot L$
000	(+)14.763 758	(+)14.763 758	(+)14.763 758
110	(+)0.917 469	(+)0.896 784	(+)0.505 599
111	(+)0.938 575	(+)0.907 006	(+)0.378 272
200	(−)0.275 791	(−)0.263 531	(−)0.082 072
211	(+)0.179 375	(+)0.167 483	(+)0.029 245
220	(+)0.267 707	(+)0.244 459	(+)0.025 407
221	(+)0.311 919	(+)0.281 478	(+)0.021 735
222	(+)0.334 889	(+)0.291 973	(+)0.010 544

TABLE VI. The scattering intensities for the G structure. The legend is the same as in Table IV.

Scattering intensities including Debye–Waller factor Gyroid structure			
hkl	$\sqrt{\langle u^2\rangle}=0$	$\sqrt{\langle u^2\rangle}=0.05\cdot L$	$\sqrt{\langle u^2\rangle}=0.25\cdot L$
000	(+)9.589 390	(+)9.589 390	(+)9.589 390
211	(+)0.428 246	(+)0.417 346	(+)0.218 318
220	(+)0.185 458	(+)0.179 281	(+)0.075 811
321	(−)0.009 438	(−)0.008 876	(−)0.001 763
332	(+)0.225 676	(+)0.205 152	(+)0.017 885
400	(−)0.113 892	(−)0.106 566	(−)0.019 556
420	(−)0.109 526	(−)0.100 557	(−)0.011 407
422	(+)0.076 736	(+)0.069 248	(+)0.005 598
431	(+)0.036 024	(+)0.032 283	(+)0.002 429
440	(−)0.009 829	(−)0.008 492	(−)0.000 044
442	(+)0.000 010	(+)0.000 008	(+)0.000 001
444	(+)0.169 050	(+)0.137 434	(+)0.000 901

$$\Lambda_{\mathrm{P,D,G}}=\frac{\left|\sum_{j=1}^{N} s_j \exp[i\mathbf{k}\mathbf{r}_j]\dfrac{\sin\left(\mathbf{k}\mathbf{n}_j\dfrac{L}{2}\right)}{\mathbf{k}\mathbf{n}_j\dfrac{L}{2}}\right|^2}{\left|\sum_{j=1}^{N} s_j \exp[i\mathbf{k}\mathbf{r}_j]\right|^2}. \tag{12}$$

Figure 2 shows a line given by the values of the function Eq. (11), for $|\mathbf{k}|$ computed in the maxima of $I_0(|\mathbf{k}|)$, Eq. (10), and interpolated between them. It has been computed for the layer width L giving the layer volume equal to 60% of the unit cell volume of the P, D, G structures. The points shown in Fig. 2 are computed by dividing the scattering intensity, including the molecular factor by the intensity for the zero width P, D, and G surfaces, Eq. (12). We remind here that in the case of the D surface the (hkl) indices have been divided by 2, as it has been explained at the begining of this section.

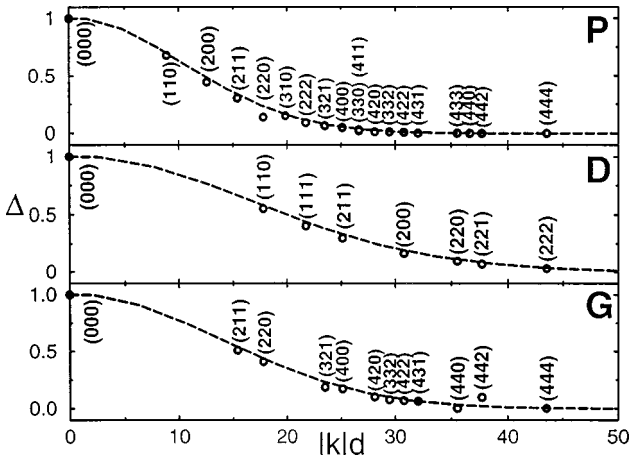

FIG. 3. The dashed lines show the functions $\Delta_S(\mathbf{k})$ [Eq. (15)] computed in the maxima of $I_0(\mathbf{k})$ [Eq. (10)] for the fluctuation amplitudes $\sqrt{\langle u^2\rangle}$ equal to 25% of the bilayer widths L. L is chosen in such a way as to give 60% of the volume fraction of surfactant in the P, D, and G structures, respectively. The ratios $\Delta_{\mathrm{P,D,G}}(\mathbf{k})$, Eq. (16), computed at the Bragg peak positions of the P, D, G structures are represented by empty circles.

It is quite surprising that the molecular form factor reduces the intensities of the Bragg peaks just like the intensity for the sphere:

$$\Lambda_S(\mathbf{k},L)\simeq\Lambda_{\mathrm{P,D,G}}(\mathbf{k},L). \tag{13}$$

Function (11) shows a quick decay with increasing $|\mathbf{k}|$. Still, intensities of the first few peaks are not reduced to zero.

The scattering intensities including the Debye–Waller factor:

$$\mathcal{F}^j_{\mathrm{DW}}=e^{-1/2(\mathbf{kn}_j)^2\langle u^2\rangle}, \tag{14}$$

are presented in Tables IV–VI. For the purpose of the analysis we have not included the molecular form factor here. In each case we compute the scattering intensities for the fluctuation amplitude equal to a certain percent of the width of the hydrocarbon part of the surfactant bilayer that occupies 60% of the unit cell volume. The data is presented only for $\sqrt{\langle u^2\rangle}$ equal to 5% and 25% of L. The Debye–Waller factor does reduce the intensities of the Bragg peaks, still this effect is fairly small. The computed peaks are at most two orders of magnitude smaller than those for a nonfluctuating surface. Again we have based the analysis of the influence of this factor on the scattering intensities for the sphere. For the Debye–Waller factor the function similar to (11) reads as

$$\Delta_S=\frac{I(\mathbf{k})}{I_0(\mathbf{k})}=\frac{\left(\int_0^\pi d\theta\sin\theta\exp[i|\mathbf{k}|\cos\theta]\exp\left[-\frac{1}{2}(|\mathbf{k}|\sqrt{\langle u^2\rangle}\cos\theta)^2\right]\right)^2}{\left(\int_0^\pi d\theta\sin\theta\exp[i|\mathbf{k}|\cos\theta]\right)^2}, \tag{15}$$

and the similar ratio for the structures P, D, and G:

$$\Delta_{\mathrm{P,D,G}}=\frac{\left|\sum_{j=1}^N s_j\exp[i\mathbf{kr}_j]\exp\left[-\frac{1}{2}(\mathbf{kn}_j)\langle u^2\rangle\right]\right|^2}{\left|\sum_{j=1}^N s_j\exp[i\mathbf{kr}_j]\right|^2}. \tag{16}$$

Functions Δ_S given by Eq. (15) and $\Delta_{\mathrm{P,D,G}}$ given by Eq. (16) are shown in Fig. 3. Again, the Debye–Waller factor reduces the scattering intensities for the TPMS just like for the sphere:

$$\Delta_S(\mathbf{k},\langle u^2\rangle)\simeq\Delta_{\mathrm{P,D,G}}(\mathbf{k},\langle u^2\rangle). \tag{17}$$

The first peaks up to 400 [(200) in the case of D] are not strongly suppressed by this factor. The function, Eq. (15), computed in the maxima of I_0 [Eq. (10)] shows a Gaussian decay, which agrees with the Gaussian form of the Debye–Waller factor. Still this decay is much slower than for the lamellar structures.[13]

Finally, we have computed the scattering spectra including both the molecular and the Debye–Waller factors. In the analysis we introduce the intensity ratio for a sphere:

$$\Omega_S=\frac{I(\mathbf{k})}{I_0(\mathbf{k})}=\frac{\left(\int_0^\pi d\theta\sin\theta\exp[i|\mathbf{k}|\cos\theta]\exp\left[-\frac{1}{2}(|\mathbf{k}|\sqrt{\langle u^2\rangle}\cos\theta)^2\right]\frac{\sin\left(|\mathbf{k}|\frac{L}{2}\cos\theta\right)}{|\mathbf{k}|\frac{L}{2}\cos\theta}\right)^2}{\left(\int_0^\pi d\theta\sin\theta\exp[i|\mathbf{k}|\cos\theta]\right)^2}, \tag{18}$$

and for the P, D, G structures:

$$\Omega_{\mathrm{P,D,G}}=\frac{\left|\sum_{j=1}^N s_j\exp[i\mathbf{kr}_j]\exp\left[-\frac{1}{2}(\mathbf{kn}_j)\langle u^2\rangle\right]\frac{\sin\left(\mathbf{kn}_j\frac{L}{2}\right)}{\mathbf{kn}_j\frac{L}{2}}\right|^2}{\left|\sum_{j=1}^N s_j\exp[i\mathbf{kr}_j]\right|^2}. \tag{19}$$

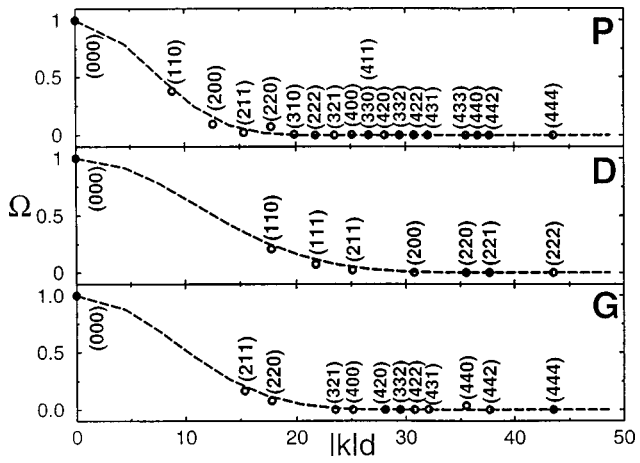

FIG. 4. The dashed lines show the functions $\Omega_S(\mathbf{k})$ [Eq. (18)] computed in the maxima of $I_0(\mathbf{k})$ [Eq. (10)] for the bilayer widths L giving 60% of the volume fraction in, respectively, the P, D, and G structures and the fluctuation amplitudes $\sqrt{\langle u^2\rangle}$ equal to 25% of L. The ratios $\Omega_{\mathrm{P,D,G}}(\mathbf{k})$ [Eq. (19)] computed at the Bragg peak positions of the P, D, G structures are represented by empty circles.

Figure 4 shows that again the Bragg peaks for P, D, and G structures are reduced according to (18):

$$\Omega_S(\mathbf{k},L,\langle u^2\rangle)\simeq\Omega_{\mathrm{P,D,G}}(\mathbf{k},L,\langle u^2\rangle). \tag{20}$$

Apart from the known TPMS (P, D, G), we have also studied the scattering spectrum of the nodal S1 surface.[14] Figure 5 shows Ω_{S1} [similar to $\Omega_{\mathrm{P,D,G}}$, Eq. (19)] calculated at the Bragg peaks of the S1 structure and the function Ω_S, Eq. (18) for a comparison. We note that in the case of two peaks (220) and (440) the intensity of the finite width, fluctuating surface is bigger than the intensity for the mathematical surface. $\Omega_{\mathrm{S1}}(220)=74.5$ and $\Omega_{\mathrm{S1}}(440)=34.4$. Still both these peaks are rather weak, $I(220)=1.788\times10^{-3}$ and $I(440)=1.025\times10^{-3}$. The intensity of the peak (400) has not been changed by the molecular form and the Debye–Waller factors. The rest of the peaks are located on the line given by Eq. (18). Even though the values of both the molecular form and the Debye–Waller factors are always smaller than one, they can increase the height of some peaks. This is caused by the fact that the scattering intensity function, Eq. (7), cannot be represented by a simple multiplication of the structure form factor, the molecular form factor, and the Debye–Waller factor.

Directions (hkl) in which the ratios $\Omega_{\mathrm{P,D,G,S1}}$ are not located near the line given by Ω_S should have a distribution of normal vectors significantly different from the distribution

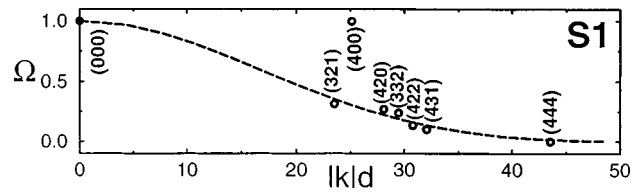

FIG. 5. The ratio $\Omega_{\mathrm{S1}}(\mathbf{k})$ [Eq. (19)]. The legend is the same as in Fig. 3.

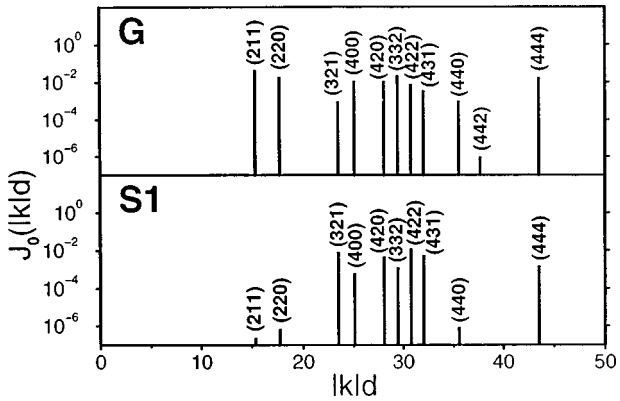

FIG. 6. The scattering intensities for the zero width, nonfluctuating G and S1 surfaces.

for a sphere and thus characteristic for the explored surface. These directions should provide useful data in the determination of the surface via the NMR studies.[22]

Figures 6 and 7 show the scattering intensities for the G and S1 structures. From Fig. 7 one sees that for the G surface the first two peaks are dominant, while in the case of the S1 structure only the higher-order peaks are large enough to be determined experimentally.

IV. SUMMARY

We have found that the influence of both the molecular form and the Debye–Waller factors can be very well modeled by the scattering function for the sphere. This analysis provides a simple mathematical tool that can faciliate examining experimental scattering data. Having an experimental scattering intensity function I_E and knowing the unit cell size d, the surfactant layer width L, and approximate fluctuation amplitude $\sqrt{\langle u^2\rangle}$ one can divide the measured scattering intensities $I_E(\mathbf{k},d,L,\langle u^2\rangle)$ by the function given by Eq. (18) to obtain the scattering intensities $J_0(\mathbf{k})$ of the zero width, mathematical surface of explored structure,

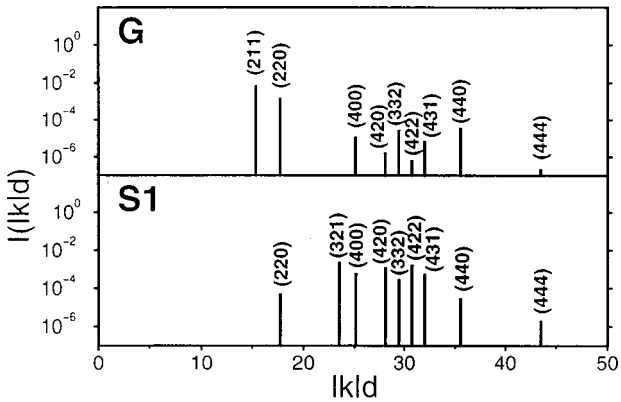

FIG. 7. The scattering intensities for finite width, fluctuating G and S1 surfaces. In both cases the width of the surface, L, is such that 60% of the volume fraction is occupied by the surfactant tails and fluctuation amplitudes $\sqrt{\langle u^2\rangle}$ are equal to 25% of L.

$$J_0(\mathbf{k}) \simeq \frac{I_E(\mathbf{k},d,L,\langle u^2\rangle)}{\Omega_S\left(\mathbf{k}d, \frac{L}{d}, \frac{\langle u^2\rangle}{d^2}\right)}. \tag{21}$$

The data of $J_0(\mathbf{k})$ is presented in the first columns of Tables I–III for the P, D, and G structures and for the S1 surface in Fig. 6.

Comparing the functions $\Omega_{\mathrm{P,D,G,S1}}$ with the function Ω_S, one can determine the directions in which the given structure has the distribution of normal vectors significantly different from the distribution for a sphere. These directions will provide NMR spectra characteristic for the given structure.

The comparison of the scattering intensities for the G and S1 structures of the same space group symmetry $Ia\bar{3}d$ suggests that complex structures have the low-order peaks very small. This effect may, in principle, cause their misdetermination.

ACKNOWLEDGMENT

This work has been supported by KBN Grant No. 2P03B12516.

[1] V. Luzzati and P. A. Spegt, Nature (London) **215**, 701 (1967).
[2] V. Luzzati, T. Gulik-Krzywicki, and A. Tardieu, Nature (London) **218**, 1031 (1968).
[3] L. E. Scriven, Nature (London) **263**, 123 (1976).
[4] P. Barois, D. Eidam, and S. T. Hyde, J. Phys. C **7**, 25 (1990).
[5] P. Strom and D. M. Anderson, Langmuir **8**, 691 (1991).
[6] P. J. Maddaford and C. Toprakcioglu, Langmuir **9**, 2368 (1993).
[7] M. H. Ropers, M. J. Stebe, and V. Schmitt, J. Phys. Chem. B **103**, 3468 (1999).
[8] M. B. Sjobom, H. Edlund, and B. Lindstrom, Langmuir **15**, 2654 (1999).
[9] E. L. Thomas, D. B. Alward, D. J. Kinning, D. C. Martin, D. L. Handlin, and L. J. Fetters, Macromolecules **19**, 2197 (1986).
[10] D. A. Hajduk, P. E. Harper, S. M. Gruner, C. C. Honeker, E. L. Thomas, and L. J. Fetters, Macromolecules **28**, 2570 (1995).
[11] A. H. Schoen, ''Infinite periodic minimal surfaces without self-intersections,'' NASA Technical Note No. D-5541, Washington, DC, U.S. GPO, 1970.
[12] W. T. Góźdź and R. Holyst, Phys. Rev. E **54**, 5012 (1996).
[13] A. L. Mackay, Nature (London) **314**, 604 (1985).
[14] D. M. Anderson, H. T. Davies, L. E. Scriven, and J. C. C. Nitsche, Adv. Chem. Phys. **77**, 337 (1990).
[15] M. Clerc and E. Dubois-Violette, J. Phys. II **4**, 275 (1994).
[16] R. Bruinsma, J. Phys. II **2**, 425 (1992).
[17] A. Aksimentiev and R. Holyst, J. Chem. Phys. **111**, 2329 (1999).
[18] R. Holyst, Phys. Rev. A **44**, 3692 (1991).
[19] U. S. Schwarz and G. Gomper, Phys. Rev. E **59**, 5528 (1999).
[20] S. T. Hyde, J. Phys. C **7**, 209 (1990).
[21] R. Holyst, D. Plewczyński, A. Aksimentiev, and K. Burdzy, Phys. Rev. E **60**, 302 (1999).
[22] W. T. Góźdź and R. Holyst, J. Chem. Phys. **106**, 9305 (1997).